Nuclear Inst. and Methods in Physics Research, A 1020 (2021) 165898

Contents lists available at ScienceDirect

Nuclear Inst. and Methods in Physics Research, A

journal homepage: www.elsevier.com/locate/nima

Lithium indium diselenide — An advanced material for neutron detection

Liviu Matei [a], Rastgo Hawrami [a], Vladimir Buliga [a], Stephen Babalola [b], Martine C. Duff [c,*], Laken Inabinet [c], Taylor Baldwin [c], Adam Jandeska [d], Arnold Burger [a]

[a] Department of Physics, Fisk University, 1000 17th Avenue North, Nashville, TN 37208, United States of America
[b] Department of Physics, Chemistry and Mathematics, Alabama A&M University, Normal, AL 35762, United States of America
[c] Savannah River National Laboratory, Aiken, SC 29808, United States of America
[d] Savannah River Nuclear Solutions, Savannah River Site, Aiken, SC 29808, United States of America

ARTICLE INFO

Keywords:
Lithium indium diselenide
Room temperature semiconductor
Thermal neutron detector

ABSTRACT

This paper describes the synthesis, crystal growth, detector fabrication, radiation hardening studies, MCNP modeling, and characterization of lithium indium diselenide or $LiInSe_2$. This newly-developed room-temperature thermal neutron detector has semiconducting and scintillating properties and it is suitable for neutron detection application. $LiInSe_2$ was synthesized starting from elemental Li, In, Se in two steps due to high reactivity of Li. A single crystal of $LiInSe_2$ was grown using the Vertical Bridgman method. The room temperature band gap was found to be 2.8 eV using optical absorption measurements. Bulk resistivity was measured at ~5 × 10^{11} Ωcm. Photoconductivity measurements of $LiInSe_2$ wafers identified a peak in the photocurrent around 445 nm. Nuclear radiation detectors were fabricated from single crystal wafer and the responses to alpha particles at various biases were measured. The mobility-lifetime product was estimated. Gamma irradiation studies were performed with calculated absorbed doses ranging from 0.2126 to 21,262 Gy. The characterization of the two wafers for their scintillator performance was conducted after each irradiation. The gamma irradiation produced a reduction of the light yield that translated to a lower channel number for the centroid of alpha detection spectra. It also showed a considerable reduction of the decay time after the first irradiation. These are the first studies on gamma radiation hardening with this material.

1. Introduction

The main material used on instruments for neutron detection was helium-3 (^{3}He). The ^{3}He isotope has an extremely low natural abundance and it is obtained as a decay product of tritium. The drastic reduction of ^{3}He isotope production [1,2] due to non-proliferation treaties has created a high demand for alternative materials. Since neutrons only interact with the nucleus, materials containing elements with high cross-sections can be used in neutron detection devices. Lithium-6 (^{6}Li, cross-section of 938 barns) [3] is one of the isotopes that meets this description. The reaction of ^{6}Li with a neutron is:

$$^6Li + n \rightarrow {}^3H + \alpha + \gamma$$

This makes the Li-containing semiconductors promising candidates for neutron detection. The ternary I–III–VI group of chalcogenides (compounds containing sulfur, selenium, or tellurium) have attracted interest because they are chemically- and physically-stable and their band gap is suitable for room-temperature radiation detection.

Kamijoh and Kuriyama [4] grew $LiInSe_2$ crystals using directional solidification. They obtained high resistivity values near 2 × 10^{11} Ωcm with a band gap of 1.88 eV at room temperature with their material. A bandgap of 2.8 to 2.86 eV was determined by Kargar et al. (2020) with 38 devices of fabricated $LiInSe_2$ material that was obtained from vertical Bridgman growth. They also calculated a resistivity values that ranged from 1 × 10^{10} to 6 × 10^{12} Ωcm and concluded that there was ohmic behavior [5]. Isaenko et al. [6] reported growth of chalcogenides crystals (including $LiInSe_2$) using the vertical Bridgman technique. They studied the effects of Li concentration and annealing on the optical properties of these crystals [7,8]. They also used a vapor of Li_2Se could be used to anneal secondary phases that formed during synthesis but this results in changes in color and in the spectra at the visible/near-IR edge energy range [6]. Belushkin et al. (2020) examined neutron detection of material grown with the vertical Bridgman–Stockbarger method using a californium-252 (^{252}Cf) source [9]. Radiation damage can have an adverse effect on material characteristics by potentially reducing light yield in scintillators whereas in semi-conductors, radiation damage can cause increases in leakage current as well as losses in energy resolution as summarized by Knoll (2010) [10]. In this work we present the synthesis, growth, fabrication, radiation hardening,

* Corresponding author.
E-mail addresses: lmatei@fisk.edu (L. Matei), Martine.duff@srnl.doe.gov (M.C. Duff).
URL: https://www.fisk.edu (L. Matei).

https://doi.org/10.1016/j.nima.2021.165898
Received 28 June 2021; Received in revised form 9 September 2021; Accepted 5 October 2021
Available online 16 October 2021
0168-9002/

Monte Carlo N-Particle (MCNP) radiation transport code analysis and characterization of $LiInSe_2$.

2. Experimentals

2.1. Synthesis of $LiInSe_2$

Synthesis of $LiInSe_2$ starts with elemental Li, indium (In) and selenium (Se). The purity of In and Se was 5N, and the Li purity was 3N. Due to the high reactivity of Li, the synthesis was conducted in two steps: forming LiIn alloy and reacting LiIn alloy with Se by vapor transport. These two steps were conducted using a pyrolithic boron nitrate (pBN) crucible. Use of pBN instead of quartz helps to avoid the reaction of Li with quartz. A small excess amount above the stoichiometric masses (3 to 4% Li and 0.5% Se) was added during the synthesis because Li and Se are more volatile than In. Crystals of $LiInSe_2$ were grown from a stoichiometric composition have a high concentration of Li-vacancies due to the high volatility of Li. The elemental Li leaving the melt is highly reactive and it will cause a degradation of the fused silica ampule. Tupitsyn et al. (2012) found that crystals grown from excess Li will grow close to the stoichiometric composition and be nearly independent on the amount of Li excess [11]. Furthermore, the addition of Se was found to lower the negative effects caused by Li reaction to the fused silica ampule. This addition did not affect the stoichiometry of $LiInSe_2$.

The LiIn alloy was formed by slowly heating the elemental Li and In beads after they were placed in a pBN crucible. The pBN crucible was then put inside a quartz ampoule and sealed in an argon (Ar) atmosphere. The LiIn alloy was melted inside the pBN crucible and allowed to react with Se vapor. After extraction from the pBN crucible under an Ar atmosphere in a Mbraun GloveBox, the synthesized material was crushed and placed in a new pBN crucible for growth. The synthesized material was crushed and placed in a tipped shaped pBN crucible inside a quartz ampoule that was sealed in Ar atmosphere. Growth was conducted in a two-zone furnace with a hot zone at 940 °C and cold zone at 780 °C. The ampoule was translated from hot to cold zone at the rate of 7 mm day^{-1}. After the entire material was crystallized, the cold zone was slowly cooled to room temperature. A wafer was harvested from the ingot and polished to 1.5 mm thickness. The wafer was polished and then etched in a 3% Br-methanol solution for 1 min. Gold (Au) contacts of 3.14 mm in diameter were deposited by RF sputtering after polishing.

2.2. Characterization of grown material without radiation hardening

A Cary 4000 UV–VIS spectrometer was used to obtain an absorption spectrum in the range of 400 to 800 nm. An optical Microscope Nikon Eclipse LV100 (20X magnification) was utilized to image the wafer by focusing the microscope at every 33 μm along the thickness of the wafer. Current–voltage (I–V) characteristics were obtained with a Keithley 237 source meter. A variable bias (0 to 100 V) was applied on the Au contacts of the wafer and the current was recorded in 20 steps. An Oriel Cornerstone 130 monochromator was used to illuminate the cathode of the wafer over a wavelength range of 200 to 1000 nm. The wafer was biased with a constant voltage of 1000 V and the current was measured for each 5 nm step of wavelength. Radiation detection tests were conducted by exposing the biased wafer to alpha particles coming from an ^{241}Am source.

2.3. Radiation hardening studies

Two additional wafers of $LiInSe_2$ were harvested for irradiation studies. Two parallel faces were polished using polishing pads of 600 to 1200 grits and a polishing paste of 3 and 0.5 μm. The two wafers were irradiated upon delivery at the gamma irradiation facility. The wafers were kept in their plastic containment for their protection during handling and irradiation. The wafers were positioned with their thinnest portion perpendicular to the gamma X-ray beam. They were irradiated at the 735-2B Gamma Beam Irradiation (GBI) Facility (Savannah River Site, Aiken, SC). A gamma exposure delivered a radiation absorbed dose of 0.21 Gy to one crystal and 2.1 Gy to the second crystal with a 6500 Ci (nominal) ^{60}Co source. After each irradiation, the crystals were characterized (described in the following section). After that examination, the crystals were returned to the irradiation facility where a radiation absorbed dose of 21.05 Gy was delivered to the first crystal (that received 0.21 Gy previously) and a second crystal (that received 2.1 Gy previously) received 210.5 Gy. Exposures that exceeded an 8-hour workday were conducted over several working days when needed. One of the crystals became damaged after the first irradiation; its size was reduced.

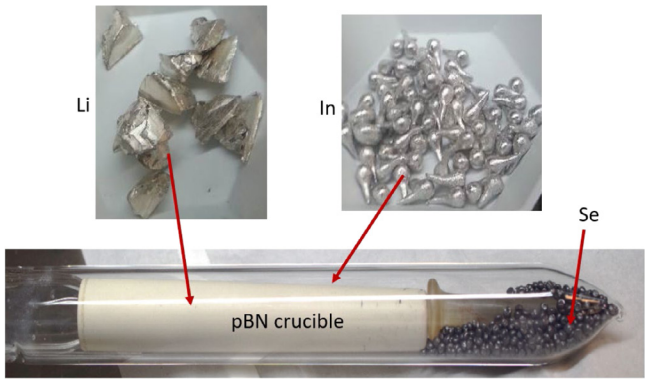

Fig. 1. The $LiInSe_2$ synthesis process and images of the reagent material.

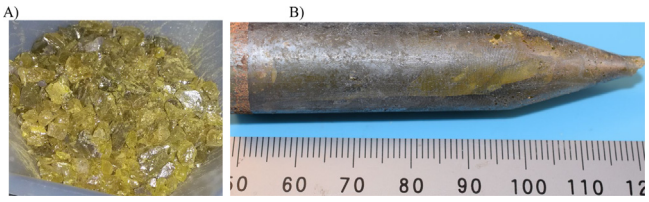

Fig. 2. (A) Synthesized $LiInSe_2$ that was crushed before loading in a new pBN crucible for growth and (B) an ingot of $LiInSe_2$ that was extracted from the pBN crucible.

Emission spectra for each treated sample was obtained using an X-ray Excited Optical Luminescence (XEOL) system. Each wafer sample was exposed a ^{241}Am alpha source and the light produced by the scintillation of $LiInSe_2$ was converted into an electrical signal by the Hamamatsu Photo Multiplier Tube (PMT). The same setup decay time (determined by averaging 100 waveforms acquired as crystals were exposed to the same source ^{241}Am) was obtained using a Picoscope 3200 oscilloscope.

2.4. Monte Carlo N-Particle (MCNP) radiation transport code studies

A MCNP 6.1 simulation was developed using a three-dimensional model of the GBI Facility to determine dose rate to a $LiInSe_2$ wafer from the 6500 Ci (nominal) ^{60}Co gamma source. The floor, ceiling, walls, source cask, lead linings, steel linings, source, beam tube, work bench were included within the geometric model. The sample to source distance was defined as 61.9 cm. Geometric objects on the boundary of the problem (i.e., walls, ceiling, and floor, outer steel and lead) were considered low impedance regions and photon interaction in these areas were considered to be outside the scope of the simulation. The source was last calibrated on November 10, 2010. It was decay-corrected based on a calibration activity of 4.172897×10^{14} photons s^{-1} [12].

Material specifications for the borosilicate glass (source container), SS-304, concrete, SS-298, and air were taken from PNNL-15870 [13].

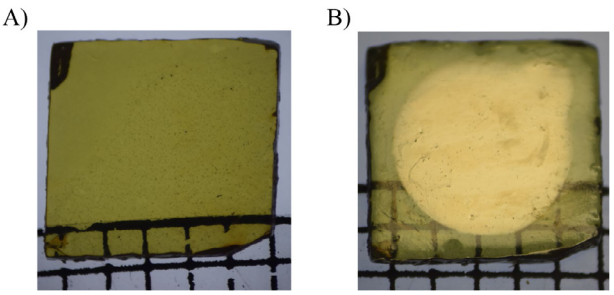

Fig. 3. A wafer of $LiInSe_2$ (A) after polishing and (B) after Au contacts were deposited by RF sputtering.

The $LiInSe_2$ material was modeled according to the mass fractions of its constituent elements. Its density was defined per crystal grower specifications at 4.26 g cm^{-3}. The simulation was run using an *F8 tally. An F6 tally for dose is typically the standard use case in MCNP, but the model makes certain assumptions: (1) charged particle equilibrium, (2) negligible radiative losses, and (3) that secondary electrons have a short range. For small cells, condition 3 is often an issue. The small volume of the $LiInSe_2$ wafer cell, 0.0133 cm ^{3}, necessitated the use of an alternative tally method. The *F8 tally is the most accurate tally for dose, but it does require substantial run time for convergence (6+ hours) and required uniform sampling of the target cell. Development of the code also utilized MCNP user guides and manuals that were produced by Los Alamos National Laboratory and Kansas State University [14,15].

3. Results and discussion

3.1. Growth, characterization and fabrication of grown material

The synthesis materials and pBN crucible are shown in Fig. 1. Fig. 2A shows the crushed synthesis material before it was loaded in the crucible prior to the growth. Fig. 2B presents an image of the ingot of $LiInSe_2$ after extraction from the pBN crucible. A small amount of bubbling was observed in the final boule (upper right portion of Fig. 2B). This is most likely due to the vapor transport of Se on the molten alloy of Li and In during the synthesis. Kargar et al. (2020) identified more intense bubbling in their material which was grown using Vertical Bridgman growth in a two-zone Mellon furnace [5]. They concluded that their formation occurred upon the melting of Li and In in the boule. Fig. 3 shows a wafer of LiInSe2 after polishing (Fig. 3A) and after (Fig. 3B) Au contacts were deposited by RF sputtering.

Tauc plots were used to determine a band gap of 2.8 eV based on UV–VIS absorption spectrum for the wafers. Fig. 4A presents a UV–VIS absorption spectrum. Fig. 4B presents the pulse height analysis spectra that was taken at three voltages. Radiation detection tests that relied on alpha particles coming from the source was used to simulate the alpha that is produced by the reaction of neutrons. This interaction with Li demonstrates an ability of the fabricated material to detect neutrons. The tests were conducted at various biases applied to the wafer which created an electric field between 3333 V cm^{-1} and 6000 V cm^{-1}.

Large secondary phases were visible in the optical image in Fig. 5A. There are many secondary phases with different sizes, but they are not visible because they are out of focus. Sequential individual images that were obtained in focus were combined as a minimum intensity projection. This approach avoids duplicate counting of large secondary phases. Fig. 5A presents a minimum intensity projection of images for every 33 μm portion of the wafer. The software associated with the microscope measures the area of each precipitate and then using a spherical approximation, the equivalent diameter and equivalent volume are calculated. The densities of secondary phases of various sizes are calculated and the volume fractions of size classes of secondary phases are determined in ppm. Secondary phases that were less than 1 μm were not counted due to limit of the camera resolution. Fig. 5B presents the density distribution of secondary phases. Fig. 6A presents the I–V characteristics of the wafer and the photocurrent vs. wavelength characteristics are shown in Fig. 6B. The most optimal FWHM obtained for alpha detection was around 38%. The mobility-lifetime product ($\mu\tau$) was estimated using the centroid channel number vs. voltage applied. The $\mu\tau$ value was around $2.5*10^{-5}$ cm $^2V^{-1}$.

3.2. Characterization of two irradiated sample materials and testing as a scintillator

An image of the two wafers that were used in the irradiation study is shown in Fig. 7. The doses to the wafers are listed in Table 1. The effect of irradiation on the optical absorbance was fairly insignificant (Fig. 8). The band gap energy did not change with irradiation based on the Tauc plots (Fig. 9) but there was a small increase in band gap for the first sample after first irradiation. Fig. 10 presents the spectra of emission for each $LiInSe_2$ samples. The peak of emission and FWHM were determined from the spectra. Repetitive measurements on the various samples of $LiInSe_2$ exposed to the same current and voltage of the X-ray tube revealed no decrease in the luminescence. The voltage and the current were chosen to optimize the measurement time which was limited by the optical spectrometer software. The emission peak wavelength varied by less than 1% of the expected value of 515 nm. The counts of emission spectra decreased as the two wafers received

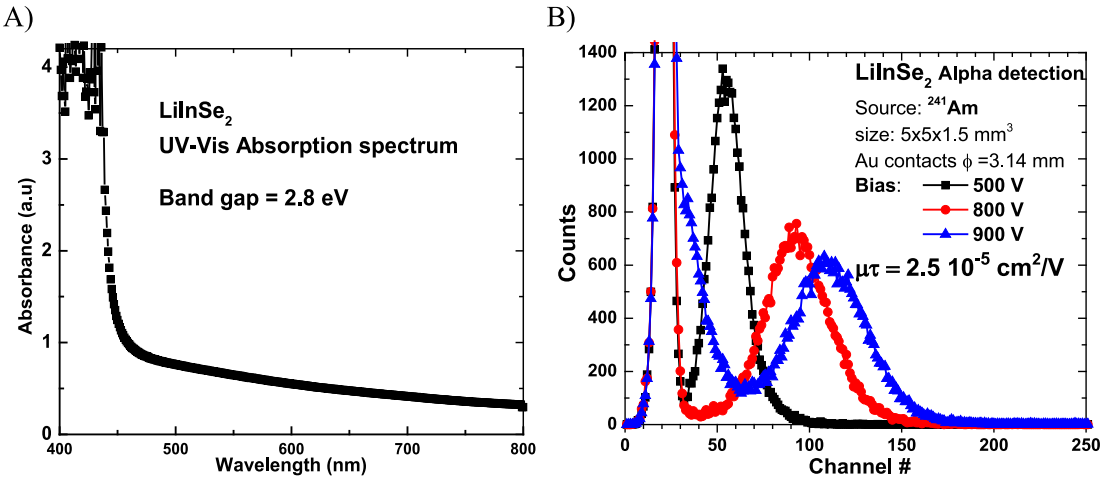

Fig. 4. (A) The UV–VIS absorption spectrum of $LiInSe_2$ and (B) its detector response of ^{241}Am alpha particle for three biases.

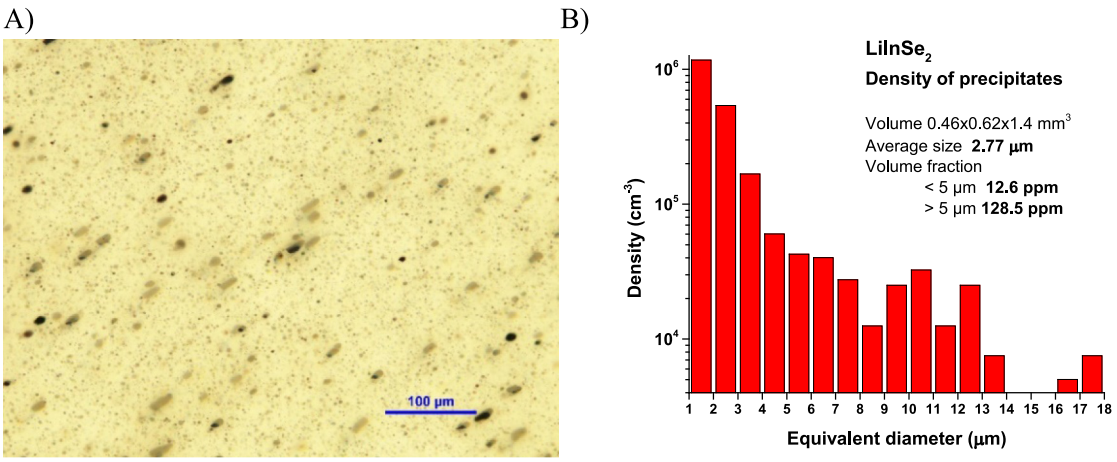

Fig. 5. (A) An optical image of the secondary phases of $LiInSe_2$ - minimum intensity projection of images taken every 33 μm along the thickness of the wafer and (B) a plot of the density of secondary phases per equivalent diameter of $LiInSe_2$ wafer.

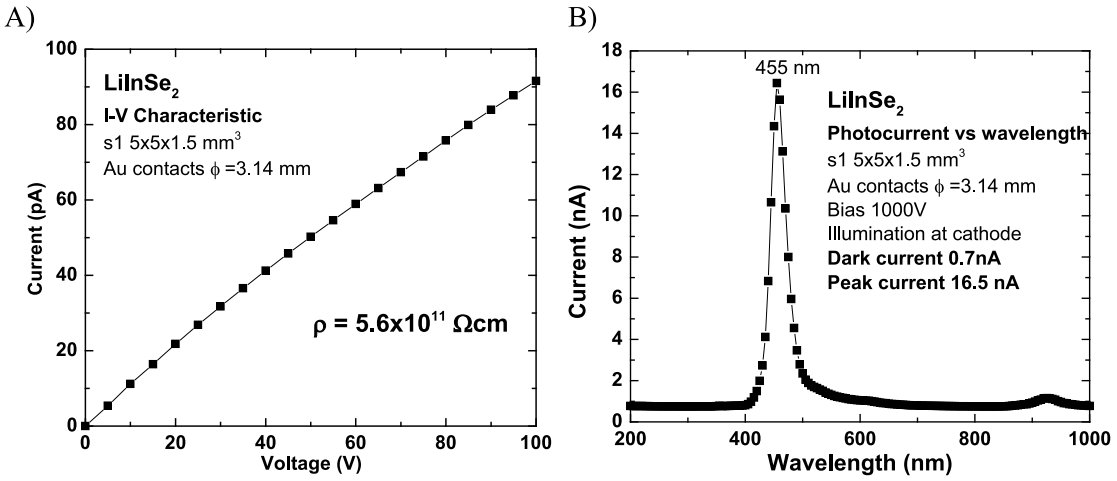

Fig. 6. (A) Current voltage characteristic of $LiInSe_2$ and (B) the photocurrent vs. wavelength characteristics with measured photocurrent peak at 455 nm for the range of 200 to 1000 nm.

increasing doses during irradiation. This suggests that a reduction of light yield occurs during the alpha radiation detection as shown in Fig. 11. Fig. 11 presents alpha detection response as a scintillator for each sample before and after each consecutive irradiation. Fig. 11 presents the acquired data before and after each irradiation and the decay time was estimated using the exponential decay fit. Radiation exposure caused the centroid of the alpha energy peak to shift to a lower energy relative to the initial untreated wafer material. The alpha decay time decreased after first irradiation and the trend in response was maintained as the irradiation steps progressed (Fig. 12). The alpha response time for the original untreated material decreased to 79% (for wafer 1) and 78% (for wafer 2) by the last radiation treatment. There was little relative decrease in decay time between the samples from the last two irradiations.

3.3. MCNP calculations for the two irradiated sample materials

The result of the *F8 tally in MCNP is designated in MeV. This absorbed dose result is normalized by the number of photons produced by the source. In our MCNP simulation there are only several billion photons produced by the source for which interactions are tracked. The energy absorption rate can be calculated as 0.014064 Gy s^{-1} using the decay corrected calibration data for the ^{60}Co source [# of photons produced second $(s)^{-1}$], and the mass of the sample (0.0566 g). This was based on the initial result of the MCNP calculation, 4.563×10^{-8} MeV,

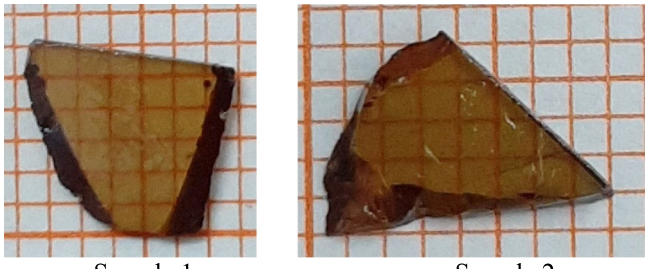

Fig. 7. Two samples of polished $LiInSe_2$ with two parallel faces.

Table 1
List of absorbed gamma radiation doses to the crystals.

Wafer number	Cumulative calculated gamma dose		
	Treatment 1	Treatment 2	Treatment 3
1	0.21 Gy	21.26 Gy	2,126.26 Gy
2	2.10 Gy	212.60 Gy	21,262.60 Gy

and a decay-corrected activity of 1.09×10^{14} photons s^{-1}. To achieve the proposed doses in Table 1, anticipated times for exposure were computed and are noted in Table 2. The statistical checks performed

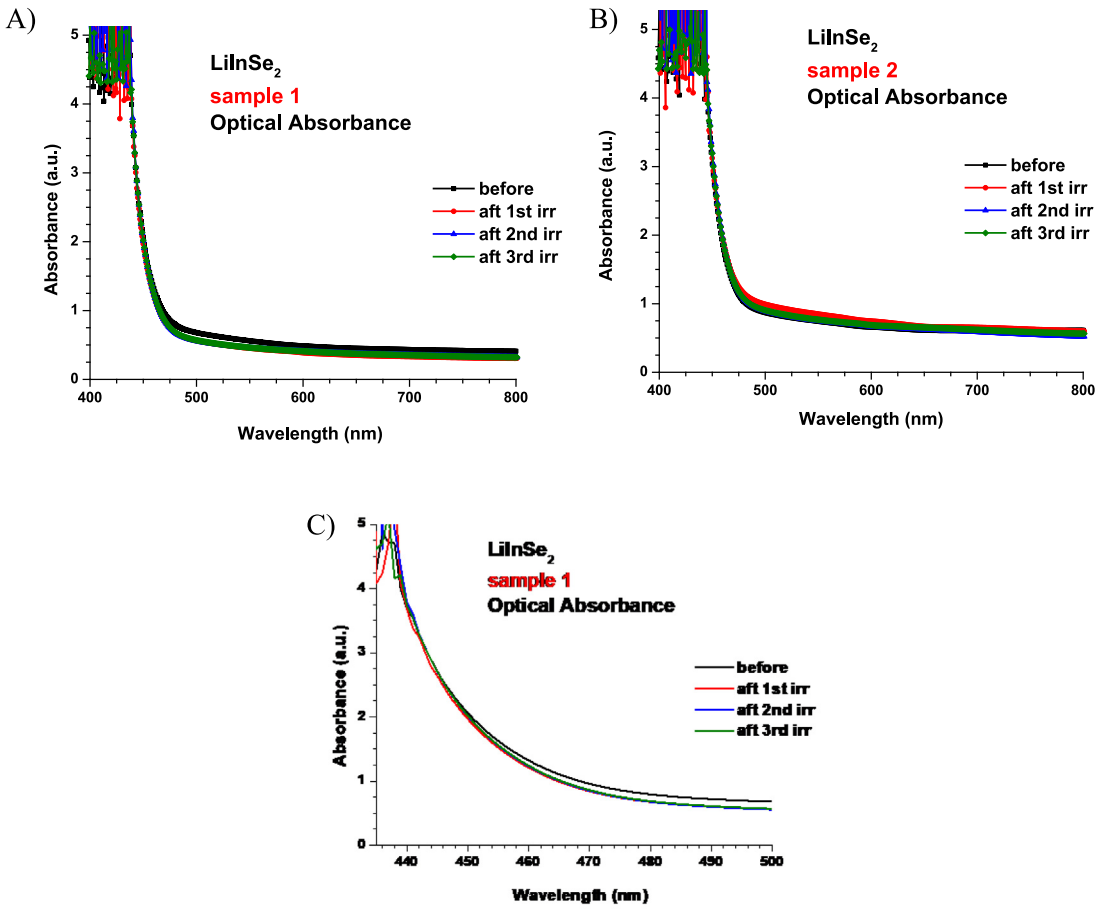

Fig. 8. Optical absorption spectra of the two $LiInSe_2$ samples before and after (aft) each irradiation (irr).

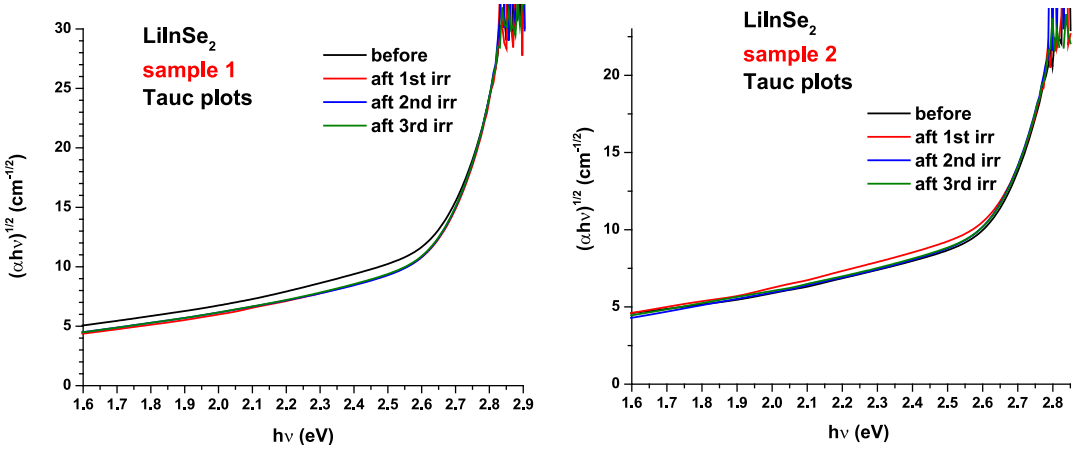

Fig. 9. Tauc plots of absorbance spectra of the two $LiInSe_2$ samples before and after each irradiation.

Table 2
Anticipated time for exposure to achieve proposed doses.

Proposed dose (Gy)	Anticipated time for exposure					
0.21262	15.11838969	s	0.251973	min	0.0042	h
2.12626	151.1838969	s	2.519732	min	0.041996	h
21.2626	1511.838969	s	25.19732	min	0.419955	h
212.626	15118.38969	s	251.9732	min	4.199553	h
2126.26	151183.8969	s	2519.732	min	41.99553	h
21262.6	1511838.969	s	25197.32	min	419.9553	h

by the MCNP code noted a relative error [1/sqrt(nps)] of less than 0.10, a variance of the variance of less than 0.02, and that all tallies passed statistical checks. These checks were to ensure that enough particles had been tracked through the sample cell (and undergone associated collisions) and thus maintain a high confidence in the statistics of the problem.

4. Conclusion

The $LiInSe_2$ semiconductor material that was synthesized had a band gap of 2.8 eV and a bulk resistivity around 5×10^{11} Ωcm.

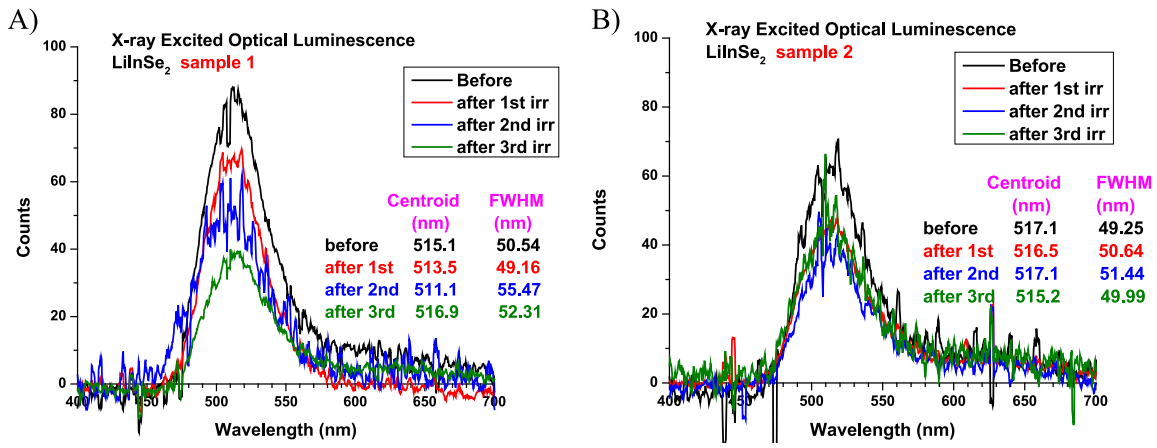

Fig. 10. $LiInSe_2$ emission spectra of the two samples measured before and after each irradiation.

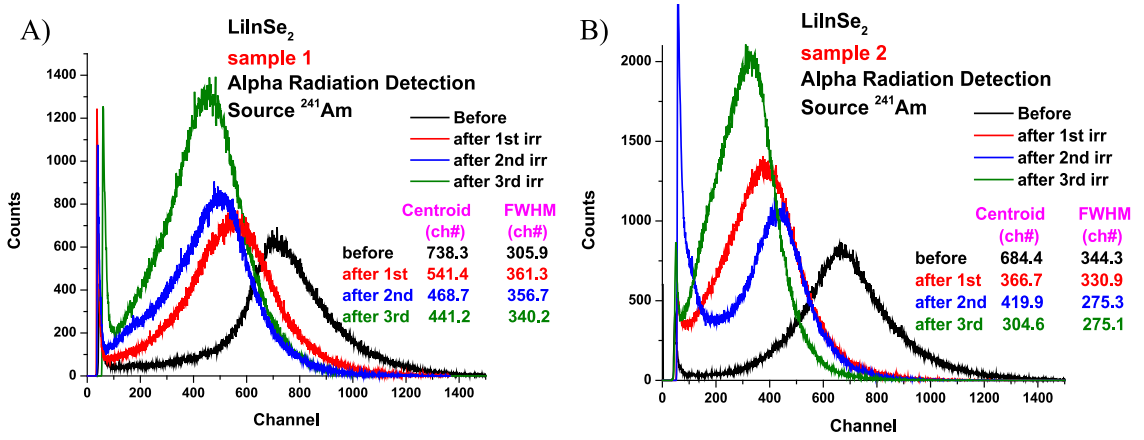

Fig. 11. Alpha radiation detection spectra of the two samples measured before and after each irradiation. Radiation exposure caused the centroid of the alpha energy peak to shift to a lower energy relative to the initial untreated wafer material.

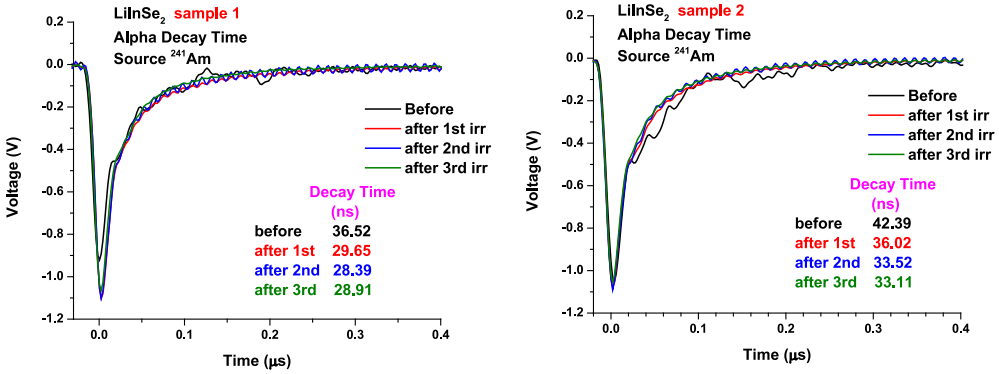

Fig. 12. Alpha radiation decay time measured of the two samples before and after each irradiation.

These properties make it appropriate for room-temperature radiation detection applications. The photocurrent of $LiInSe_2$ is well pronounced at 445 nm, which indicates there is a reasonable generation rate and mobility of the charge carriers. The detection response tests proved that $LiInSe_2$ semiconductor could detect alpha particles produced by the reaction of Li with neutrons. The mobility-lifetime product that was determined is highly appropriate for the intended detector applications. The characterization of the two wafers after each irradiation proved that the gamma irradiation produced a reduction of the light yield, which may preclude the use of this material in high radiation backgrounds. This reduction in light translated to a lower channel number for the centroid of alpha detection spectra. It also demonstrated a reduction of the decay time after the first irradiation, which continued as the irradiation steps progressed. These are the first studies on gamma radiation hardening with this material to our knowledge.

Additional studies are needed to better explain the decrease in scintillation detector performance after gamma irradiation. Follow-on studies that explore the use of annealing to remove radiation damage could prove useful. Studies could also be conducted that focus on changing the stoichiometry of the starting materials. This could reduce the formation of secondary phases and help improve material performance.

CRediT authorship contribution statement

Liviu Matei: Data acquisition, Naterial synthesis and preparation. **Rastgo Hawrami:** Data acquisition, Material synthesis and preparation. **Vladimir Buliga:** Data acquisition, Material synthesis and preparation. **Stephen Babalola:** Conceptualization, Project administration, Funding acquisition. **Martine C. Duff:** Funding acquisition, Project administration, Writing and editing. **Laken Inabinet:** Data acquisition, Irradiation treatments. **Taylor Baldwin:** MCNP data curation. **Adam Jandeska:** Irradiation treatments. **Arnold Burger:** Conceptualization, Project administration, Funding acquisition.

Declaration of competing interest

The authors declare that they have no known competing financial interests or personal relationships that could have appeared to influence the work reported in this paper.

Funding

This work was supported in part by : U.S. Dept. of Energy/Savannah River Nuclear Solutions, LLC, Grant: DE-AC09-08SR22470, U.S. Dept. of Homeland Security, Grant #: 4300084191; U.S. ARMY, Grant #: W911NF-1–0196, and National Science Foundation, United States of America (Grant #: 0932038).

Appendix A. Supplementary data

Supplementary Material includes a copy of the MCNP code that was used to model the absorbed gamma dose to the crystal. The code was implemented to determine the time required to obtain each planned dose for a $LiInSe_2$ sample. The calculated absorbed doses are specified in Table 1.

Supplementary material related to this article can be found online at https://doi.org/10.1016/j.nima.2021.165898.

References

[1] R.T. Kouzes, The^{3}He Supply Problem, Report Pacific Northwest National Laboratory. PNNL-18388, U.S. Dept. of Energy, 2009.
[2] M.I. Wald, Shortage slows a program to detect nuclear bombs, 2009, NYtimes.com.
[3] P. Rinard, Passive nondestructive assay of nuclear materials. Chapter 12, in: Neutron Interactions with Matter. Nucl. Reg. Comm, 1991, p. 357, (NUREG/CR-5550, LA-UR-90-732).
[4] T. Kamijoh, K. Kuriyama, Single crystal growth and characterization of $LiInSe_2$, J. Appl. Phys. 52 (1981) 1102.
[5] A. Kargar, H. Hong, J. Tower, A. Gueorguiev, H. Kim, L. Cirignano, J.F. Christian, M.R. Squillante, K. Shah, $LiInSe_2$for semiconductor neutron detectors, Front. Phys. 09 (2020) http://dx.doi.org/10.3389/fphy.2020.00078.
[6] L. Isaenko, I. Vasilyeva, A. Merkulov, A. Yelisseyev, S. Lobanov, Growth of new nonlinear crystals LiMX2 (M=Al, In, Ga; X=S, Se, Te) for the mid-IR optics, J. Cryst. Growth 275 (2005) 217–223.
[7] L. Isaenko, A. Yelisseyev, S. Lobanov, V. Petrov, F. Rotermund, G. Slekys, J.-J. Zondy, $LiInSe_2$: A biaxial ternary chalcogenide crystal for nonlinear optical applications in the midinfrared, J. Appl. Phys. 91 (12) (2002).
[8] L. Isaenko, A. Yelisseyev, S. Lobanov, P. Krinitsin, V. Petrov, J.-J. Zondy, Ternary chalcogenides LiBC2 (b=in, ga; c=s, se, te) for mid-IR nonlinear optics, J. Non-Cryst. Solids 352 (2006) s23–25.
[9] A.V. Belushkin, A.A. Bogdzel, A.A. Goloshumova, L.I. Isaenko, S.I. Lobanov, V.M. Milkov, A. Yu. Tarasova, A.P. Yelisseyev, Study of $LiInSe_2$single crystals for thermal neutron detection, J. Synch. Investig. (2020) http://dx.doi.org/10.1134/s102745102007006x.
[10] G.F. Knoll, Radiation Detection and Measurement, Fourth edition, John Wiley and Sons Inc., pp. 397-399.
[11] E. Tupitsyn, P. Bhattacharya, E. Rowe, L. Matei, M. Groza, B. Wiggins, A. Burger, A. Stowe, Single crystal of $LiInSe_2$semiconductor for neutron detector, Appl. Phys. Lett. 101 (2012) 202101, http://dx.doi.org/10.1063/1.4762002.
[12] M. Hogue, Uncertainty Evaluation of^{137}Cs and ^{60}Co Exposure in the Gamma Beam Irradiator, Savannah River Site, Health-Physics Services—Radiological Engineering, 2017, p. 17, SRNS-J6700-2017-00137.
[13] R.J. McConn Jr., C.J. Gesh, R.T. Pagh, R.A. Rucker, R.G. Williams III, Radiation portal monitor project: Compendium of material composition data for radiation transport modeling, Rev. 1 (4) (2011).
[14] C.J. Werner (Ed.), MCNP Users Manual - Code Version 6.2, report LA-UR-17-29981, Los Alamos National Laboratory, 2017.
[15] J.K. Shultis, R.E. Faw, An MCNP Primer, Kansas State University, Manhattan, 2011.